arXiv:1601.04142v3 [hep-ph] 10 May 2016

May 7, 2016

Test of the triple Higgs boson form factor in $\mu^-\mu^+ \to HH$.

G.J. Gounaris[a] and F.M. Renard[b]

[a]Department of Theoretical Physics, Aristotle University of Thessaloniki,
Gr-54124, Thessaloniki, Greece.

[b]Laboratoire Univers et Particules de Montpellier, UMR 5299
Université Montpellier II, Place Eugène Bataillon CC072
F-34095 Montpellier Cedex 5.

Abstract

We study the sensitivity of the process $\mu^-\mu^+ \to HH$ to the q^2-dependence of the HHH form factor, which can reflect the Higgs boson structure, especially in the case of compositeness. We compute the Born and 1-loop SM contribution to this process. We then show how the $\mu^-\mu^+ \to HH$ polarized and unpolarized cross sections are modified by the presence of various types of anomalous contributions to the HHH form factor, in particular Higgs constituents in the case of compositeness.

PACS numbers: 12.15.-y, 12.60.-i, 14.80.-j

1 Introduction

In spite of the discovery [1] of the Higgs boson [2], as expected in the standard model (SM) [3], the SM cannot be the last word, and physics beyond SM (BSM) should exist [4]. A review on Higgs physics is for example made in [5]. In respect of BSM various types of proposals have been made leading for example to anomalous Higgs boson couplings [6, 7] or to couplings of the Higgs boson to new visible or invisible particles [8], particularly in the case of Higgs boson compositeness [9, 10, 11, 12, 13].

There are many processes (involving Higgs boson production or decay) where such Higgs boson couplings, differing from SM predictions, could be observed. However, in most of them the Higgs boson is on-shell and such a departure could not obviously tell whether it is caused by Higgs compositeness. This is particularly the case if the Higgs boson is coupled to an invisible sector.

The observation of a suitable Higgs boson form factor though, could give an answer to such questions. Indeed a composite particle (like the proton or the pion) should have a form factor. But contrarily to the case of the proton and the pion, we do not have a γHH or a ZHH vertex for studying the H form factor.

In this paper we concentrate on the HHH form factor; that is at a $q^2 \equiv s$ dependence of the HHH vertex when one H, with momentum q, is off-shell. The scale of this dependence could be in the TeV range, see e.g. [9].

There are various processes which involve the HHH coupling, but not necessarily the form factor with one H far off-shell, in which we are interested. Such processes at LHC are $gg \to H \to HH$ (with g denoting a gluon) or $ZZ \to H \to HH$, $W^+W^- \to H \to HH$ [14]; but these require complex theoretical and experimental analyses, before reaching the structure of the HHH coupling. Similarly, the $\gamma\gamma \to H \to HH$ process also involves a complex initial 1-loop H coupling related to the HHH form factor.

The simplest process directly sensitive to an HHH form factor effect, is then probably $\mu^-\mu^+ \to HH$, observable at a future $\mu^-\mu^+$ collider [15]. Even if this will be realizable only in a far future and under the condition of obtention of a very high luminosity, this process is particularly interesting because in non standard Higgs models, the $H\mu\mu$ coupling may still be similar to the SM one, whereas the Higgs boson self-coupling and the Higgs boson couplings to heavy fermions may be very different, see e.g. [11].

So below we analyze $\mu^-\mu^+ \to HH$ in this spirit. We start by computing the SM Born and 1-loop contributions to the helicity amplitudes and cross sections. At Born level they are due to s-channel H exchange and (at a weaker level) to t and u channel μ exchange. At 1-loop level, the corrections involve various triangles, boxes as well as μ and H self-energy bubbles. Some of these terms (the "right triangles" and the "bubbles with 4-leg couplings and H self-energy diagrams") already create contributions to the HHH form factor from the usual scalars, fermions and gauge boson loops, but they are relatively small, at order α. We collect them in the appendix and we illustrate their corresponding (modest) s dependence.

We then compute examples of new contributions which could be induced either by

Higgs boson compositeness or by the couplings of the Higgs boson to a new set of particles. Illustrations show how such contributions can generate spectacular differences in the s dependence of the HHH form factor, with respect to the one predicted by the SM.

These different 1-loop corrections reflect in the various amplitudes and cross sections and could be useful for guessing what type of contribution is necessary in order to explain a possible departure of the measurements with respect to the SM expectation. We separately consider the helicity conserving (HC) and the helicity violating (HV) amplitudes and the polarized cross sections, as these ones may be measurable in this process [16].

Contents: Section 2 is devoted to the presentation of the SM Born amplitudes and cross sections of the $\mu^-\mu^+ \to HH$ process and Section 3 to the SM 1-loop contributions. Examples of anomalous HHH contributions effects are described in Section 4. In the concluding Section 5 we summarize our results and we mention that this type of study of the effect of the HHH form factor could also be done in several other (but more complex) HH production processes.

2 SM Born amplitudes and cross sections

The SM Born amplitude of the $\mu^-\mu^+ \to HH$ process is due to 3 diagrams: the s channel H exchange with an initial $(\mu^-\mu^+H)$ and a final (HHH) coupling, and two diagrams with t and u channel $\mu^\mp$ exchange with up and down $(\mu^-\mu^+H)$ couplings. The invariant Born amplitude is

$$\begin{aligned} A^{\rm Born}(\mu^-\mu^+ \to HH) = & -\frac{e^2 g_{\mu\mu H} g_{HHH}}{s - m_H^2 + i m_H \Gamma_H} \bar{v}(l',\lambda') u(l,\lambda) \\ & -e^2 g_{\mu\mu H}^2 \left[\frac{\bar{v}(l',\lambda')(\not{q}' + m_\mu) u(l,\lambda)}{t - m_\mu^2} + \frac{\bar{v}(l',\lambda')(\not{q}'' + m_\mu) u(l,\lambda)}{u - m_\mu^2} \right] \ , \end{aligned} \tag{1}$$

where (λ, λ') are the (μ^-, μ^+) helicities, (l, l', p, p') are the (μ^-, μ^+, H, H) momenta and we also define

$$\begin{aligned} & q = l + l' \ , \ q' = l - p = p' - l' \ , \ q'' = l - p' = p - l' \ , \\ & s = q^2 \ , \ t = q'^2 \ , \ u = q''^2 \ , \end{aligned} \tag{2}$$

and the couplings

$$g_{\mu\mu H} = -\frac{m_\mu}{2 s_W m_W} = -\frac{m_\mu}{ev} \quad , \quad g_{HHH} = -\frac{3 m_H^2}{2 s_W m_W} = -\frac{3 m_H^2}{ev} \ , \tag{3}$$

where the final HH are symmetrized.

The corresponding Born helicity amplitudes are

$$F^{\rm Born}_{\lambda,\lambda'}(s,\theta) = \frac{e^2 g_{\mu\mu H} g_{HHH}}{s - m_H^2 + i m_H \Gamma_H} \sqrt{s} \delta_{\lambda,\lambda'}$$
$$+e^2 g^2_{\mu\mu H} \left[\frac{1}{t - m_\mu^2} - \frac{1}{u - m_\mu^2} \right] (2\lambda) p_H \sqrt{s} \sin\theta \delta_{\lambda,-\lambda'} \quad , \tag{4}$$

where $p_H = \sqrt{s/4 - m_H^2}$, and θ is the c.m. scattering angle between l and p. Note that we computed them from the invariant amplitude in (1) by neglecting the $m_\mu/\sqrt{s}$ terms appearing in the μ propagator and in the precise expressions of the Dirac spinors. These Born amplitudes are already factorized by one or two $g_{\mu\mu H}$ couplings proportional to m_μ/m_W, so that there is no need for keeping these negligible corrections.

Note also that s-channel part in (4) is angle-independent and purely helicity violating (HV), due to the $\delta_{\lambda,\lambda'}$ term, which violates the high energy helicity conservation rule $\sum \lambda_{in} = \sum \lambda_{fin}$ [17]. This term dominates at low energy though, but it decreases like $1/\sqrt{s}$ as the energy increases.

The t and u channel parts are purely helicity conserving (HC), when neglecting $m_\mu/\sqrt{s}$ terms. They tend to a constant at high energy and are forward-backward antisymmetric (vanishing at $\pi/2$). They are about 100 times weaker than the s-channel part though, because of their additional small $g_{\mu\mu H}$ coupling factor.

So finally the only non negligible Born amplitudes are the HV ones (i.e. those due to the s-channel H exchange) in which we are interested, because of their proportionality to the HHH coupling. This is the first remarkable feature of the $\mu^-\mu^+ \to HH$ process.

The cross section for unpolarized $\mu^\mp$ beams is

$$\frac{d\sigma}{dcos\theta} = \frac{p_H}{64\pi s\sqrt{s}} \sum_{\lambda,\lambda'} |F_{\lambda,\lambda'}(s,\theta)|^2 \quad . \tag{5}$$

Cross sections with left-handed or right-handed polarized $\mu^\mp$ beams will also be considered. Note that due to the final HH symmetrization, the cross sections are necessarily forward-backward symmetric.

3 SM 1-loop contributions.

The 1-loop corrections to the above Born terms contain various types of diagrams; triangle diagrams for initial and final vertices and H self-energy bubbles for s-channel H exchange; triangle diagrams for up or down vertices and $\mu^\mp$ self-energy bubble for t, u channel $\mu^\mp$ exchange; several types (direct, crossed and twisted) of box diagrams. Some of the triangles and bubbles are divergent and a choice of renormalization scheme has to be made, consisting in the addition of specific counter terms canceling these divergences. There are various schemes for this, which differ by their choice of experimental inputs,

see [18]. One may for example use the on-shell (OS) scheme; a special application to SM and MSSM Higgs couplings is done in [19].

However in the present study we are essentially interested in the s dependence of the HHH vertex (to be then compared with possible new physics effects) and not in its precise renormalized on-shell value which will be difficult to measure accurately anyway. For this purpose we will compute the various 1-loop terms in the SRS scheme [20] which give simple high energy expressions, whose contents are immediately readable and instructive, in particular for suggesting possible models for new contributions.

We next list the various diagrams and their relative importance.
(a) In the s-channel sector we find:

(a1) Left triangles

$$(W\nu W), (Z\mu Z), (\mu Z\mu), (G\nu G), (G^0\mu G^0), (H\mu H), (\mu G^0\mu), (\mu H\mu) \ ,$$

followed by s-channel H exchange and a final HHH coupling.

(a2) Left triangles connected to the final HH by a 4leg coupling

$$(W\nu W)+(WWHH) \ , \ (Z\mu Z)+(ZZHH) \ , \ (G\nu G)+(GGHH) \ ,$$
$$(G^0\mu G^0)+(G^0G^0HH) \ , \ (H\mu H)+(HHHH) \ .$$

Denoting by $T^{\rm SM}_{\rm left}$ the sum of the a1 and a2 diagrams, the implied helicity amplitude is written as

$$F^{\rm left\ SM}_{\lambda,\lambda'} = \frac{eT^{\rm SM}_{\rm left}(s) g_{HHH}}{s-m_H^2+im_H\Gamma_H}\sqrt{s}\delta_{\lambda,\lambda'} \quad , \tag{6}$$

which is HV, like the s-channel Born terms, but is numerically small (100 to 1000 times smaller than Born, as expected from the α factor occurring for an 1-loop correction without special enhancement effect).

(a3) H self-energy and right triangles.
The implied amplitude consists of two parts. The first part $T_{\rm se}(SM)$ involves an initial $(\mu\mu H)$ coupling followed by H self-energy bubbles and a final g_{HHH} coupling. The second part, $T_{\rm tri}(SM)$, involves an initial $(\mu\mu H)$ coupling followed by H s-channel exchange and either an SM HHH form factor, or a bubble and a 4leg coupling to HH. The sum of these 2 parts

$$T^{SM}_{HHH}(s) = T_{\rm se}(SM) + T_{\rm tri}(SM) \quad , \tag{7}$$

leads to the helicity amplitude

$$F^{\rm HHH\ SM}_{\lambda,\lambda'} = \frac{eg_{\mu\mu H}T^{SM}_{HHH}(s)}{s-m_H^2+im_H\Gamma_H}\sqrt{s}\delta_{\lambda,\lambda'} \quad , \tag{8}$$

which, as (6), is also HV and angle-independent. The long list of contributions to T^{SM}_{HHH} is collected in the Appendix. It is found that, above the tt threshold, it is largely dominated

by the ttt contribution. Numerically, the amplitude in (8) contains important real and imaginary parts, comparable to the HV Born terms in[1] (4).

We next turn to **(b) in the t, u sectors** where we find:

(b1) up or down triangles with $\mu^{\mp}$ exchange:

$$(\nu WW)\ ,\ (\mu ZZ)\ ,\ (\mu HH)\ ,\ (\nu GG)\ ,\ (\mu G^0G^0)\ ,\ (Z\mu\mu)\ ,\ (H\mu\mu)\ ,\ (G^0\mu\mu)\ .$$

Among them, non negligible contributions only come from the (νWW) and (μZZ) triangles, which produce HV contributions (still 100 times weaker than the Born ones) and tending to an angular symmetric constant at high energy. The other terms lead essentially to small HC amplitudes, like the corresponding Born ones in (4).

(b2) $\mu^{\mp}$ self-energy bubbles
These t and u channel μ exchanges which were already small at Born level lead to very small HC contributions when μ self-energy bubbles are added.

Finally, the **(c) Boxes** are of two types: The direct boxes

$$(\nu WWW)\ ,\ (\mu ZZZ)\ ,\ (\nu GGG)\ ,\ (\mu G^0G^0G^0)\ ,\ (\mu HHH)\ ,\ (Z\mu\mu\mu)\ ,\ (H\mu\mu\mu)\ ,\ (G^0\mu\mu\mu)\ ,$$

and the corresponding crossed ones; the twisted boxes

$$(Z\mu\mu Z)\ ,\ (H\mu\mu H)\ ,\ (G^0\mu\mu G^0)\ ,$$

and the corresponding crossed ones. Among them, the important contributions come from (νWWW), (μZZZ) and their crossed boxes, because of the presence of W, Z couplings and the total absence of suppressed $H\mu\mu$ couplings. The induced invariant amplitudes are then given by

$$\begin{aligned} A_{\nu WWW} &= -2\alpha^2 g^2_{WWH} g^2_{W\mu L}\{-m_\mu D_{11} I_{1L} + I_{1pL}(D_{12} - D_{13})\}\ , \\ A_{\mu ZZZ} &= \alpha^2 g^2_{ZZH}\Big\{4m_\mu g_{Z\mu L} g_{Z\mu R} I_1 D_0 - 2\Big[- m_\mu D_{11}(g^2_{Z\mu L} I_{1L} + g^2_{Z\mu R} I_{1R}) \\ &\quad + (g^2_{Z\mu L} I_{1pL} + g^2_{Z\mu R} I_{1pR})(D_{12} - D_{13})\Big]\Big\}\ , \end{aligned} \tag{9}$$

written in terms of Passarino-Veltman D-functions [21], and the helicity forms decomposed as

$$\begin{aligned} I_1 = \bar v(l',\lambda') P_L u(l,\lambda) &\ \to\ -\sqrt{s}\delta_{\lambda,\lambda'}\ , \\ I_{1L} = \bar v(l',\lambda') P_L u(l,\lambda) &\ \to\ -\sqrt{s}\delta_{\lambda,\lambda'}\delta_{\lambda,-}\ , \\ I_{1R} = \bar v(l',\lambda') P_R u(l,\lambda) &\ \to\ -\sqrt{s}\delta_{\lambda,\lambda'}\delta_{\lambda,+}\ , \end{aligned} \tag{10}$$

[1]Note that the SRS scheme [20], is globally satisfactory above $\sim$ 1TeV.

for the HV contributions which are suppressed by m_μ factors, and

$$\begin{aligned} I_{1p} = \bar{v}(l',\lambda')\not{p}u(l,\lambda) &\rightarrow -p_H\sqrt{s}\sin\theta\delta_{\lambda,-\lambda'}(\delta_{\lambda,-}-\delta_{\lambda,+}) \ , \\ I_{1pL} = \bar{v}(l',\lambda')\not{p}P_Lu(l,\lambda) &\rightarrow -p_H\sqrt{s}\sin\theta\delta_{\lambda,-\lambda'}\delta_{\lambda,-} \ , \\ I_{1pR} = \bar{v}(l',\lambda')\not{p}P_Ru(l,\lambda) &\rightarrow p_H\sqrt{s}\sin\theta\delta_{\lambda,-\lambda'}\delta_{\lambda,+} \ , \end{aligned} \tag{11}$$

for the HC contributions. In (9), the couplings

$$\begin{aligned} g_{W\mu L} = \frac{1}{s_W\sqrt{2}} \ , \ g_{Z\mu L} = -\frac{1-2s_W^2}{2s_Wc_W} \ , \ g_{Z\mu R} = \frac{s_W}{c_W} \ , \\ g_{WWH} = \frac{m_W}{s_W} \ , \ g_{ZZH} = \frac{m_Z}{s_Wc_W} \ , \end{aligned} \tag{12}$$

are used. Notice that the HC amplitudes of these boxes do not involve any mass suppressed coupling constant, such that they are only reduced by the one loop α/π factor. For comparison the Born HC amplitudes (due to t,u channels $\mu^\mp$ exchange) are reduced by the factor $(m_\mu/m_W)^2$. Due to these features the box HC amplitudes are $(\frac{\alpha}{\pi})(\frac{m_W}{m_\mu})^2 \sim 1000$ times larger then the HC Born ones and have a size almost comparable to the Born HV amplitudes. Both real and imaginary parts are important.

The remaining box HV contributions coming from m_μ terms do not have this enhancement and get the usual α/π reduction factor as compared to the Born terms.

Resulting total SM amplitudes and cross sections.
These are constructed by summing the various 1-loop contributions and adding them to the Born ones. The important terms are the HV Born term of (4), the H self-energy and HHH right triangles of (8) coming essentially from top quark diagrams (see Appendix), and the aforementioned contribution from the two boxes leading to (9).

These final complete 1-loop results (Born + 1-loop diagrams) for the HC and HV SM helicity amplitudes are illustrated in Fig.1, where we show their energy and angle dependencies. Note that these complete SM HC and HV amplitudes have comparable sizes, although their s- and θ-dependencies are rather different. In particular the two HC amplitudes almost coincide at 0.5 TeV (upper right panel), which also happens for the HV amplitudes at $\theta = 60^\circ$, in a wide range of energies (lower left panel).

The corresponding (complete 1-loop) cross sections, shown in Fig.2, reflect the properties of the unpolarized cross sections defined in (5), and the $\mu^\mp$ polarized cross sections denoted as $d\sigma_{\lambda\lambda'}/d\cos\theta$. For the later, the alternative notation indicating whether the contributing amplitudes are HV or HC may also be inspiring:

$$d\sigma_{LL} \equiv d\sigma_L(HV) \ , \ d\sigma_{RR} \equiv d\sigma_R(HV) \ , \ d\sigma(HV) \equiv d\sigma_L(HV) + d\sigma_R(HV) \ , \tag{13}$$

$$d\sigma_{LR} \equiv d\sigma_L(HC) \ , \ d\sigma_{RL} \equiv d\sigma_R(HC) \ , \ d\sigma(HC) \equiv d\sigma_L(HC) + d\sigma_R(HC) \ . \tag{14}$$

As seen in Fig.2 the HV differential cross sections are angularly constant at $\sqrt{s} = 0.5$TeV and reflect mainly the s-channel H exchange parts containing the effect of the HHH form

factor. On the contrary, the HC cross section has a specific angular shape; it starts with smaller values at low energy, but becomes of comparable size to the HV one at high energies, due to the large box contributions.

The unpolarized cross section contains all these features but obviously does not allow their easy disentangling.

4 Anomalous HHH contributions

We are now looking for possible effects of a modification of the SM HHH form factor due to new physics contributions. They will only affect the HV helicity amplitudes according to the H exchange diagram, giving

$$\delta F_{\lambda,\lambda'} = \frac{e g_{\mu\mu H} \delta T_{HHH}(s)}{s - m_H^2 + i m_H \Gamma_H} \sqrt{s} \delta_{\lambda,\lambda'} \quad , \tag{15}$$

where $\delta T_{HHH}(s)$ is the departure to the SM prediction $T^{SM}_{HHH}(s)$ in (7), which is induced by the H self-energy and HHH form factor discussed in the **a3** part of Section 3.

Examples of new physics contributions
Our aim is not to study particular new models but only to look at the sensitivity of the $\mu^-\mu^+ \to HH$ process to modifications of the SM g_{HHH} coupling and especially to the s dependent form factor that they generate.

Modifications are often described by effective operators, see [6, 7]. There are various types of dimension-6 operators leading to anomalous couplings. Among them we can mention the ones generating direct effective $\mu\mu HH$ couplings like

$$O = \frac{c}{\Lambda^2} (H^\dagger \overleftrightarrow{D_\mu} H)(\bar{\mu}\gamma^\mu P_{L,R}\mu) \tag{16}$$

which would add global contributions to the $\mu^-\mu^+ \to HH$ amplitude of the type

$$c\frac{s}{\Lambda^2} v(l',\lambda')(\not{p}' - \not{p}) P_{L,R} u(l,\lambda) \tag{17}$$

as long as $s \ll \Lambda^2$, where Λ is an effective new physics scale .
More closely related to our study of the HHH form factor there is also a dimension 6 operator

$$O_T = \frac{c_T}{2\Lambda^2} (H^\dagger \overleftrightarrow{D_\mu} H)^2 \quad , \tag{18}$$

which would give an additional contribution $\delta T_{HHH}(s)$ to the standard HHH coupling of the type $c_T(s/\Lambda^2)$.

However these descriptions only parameterize a departure from the SM prediction as long as $s \ll \Lambda^2$ but not a complete s dependence (the shape) of the form factor which is our purpose.

We therefore come back to the precise structure of the HHH vertex. With the idea of compositeness we can take as example the hadronic structure of the $\sigma\sigma\sigma$ vertex where the σ is a $q\bar{q}$ bound state. This vertex can be pictured through a triangular quark loop, but it is obviously affected by non perturbative binding interactions. With such a picture the whole HHH coupling should then come from (XXX) triangles made by the constituents X and an effective HXX coupling related to the binding. This would generate an effective HHH vertex replacing the usual SM HHH Born term. On another hand, if the Higgs boson is connected to a new sector, one may have triangles involving the corresponding new particles. In the case of a strong sector (similarly to the hadronic case), there may be resonances R leading to HHH contributions of the type $H \to R(XX) \to HH$.

In Fig.3 we give illustrations of the contributions to the (HHH) form factor corresponding to such examples and we compare them to the total SM one (essentially controlled by the ttt triangle) and to its supersimplicity approximation (called sim) given in the **a3** part of Section 3.

- For a scalar Higgs-constituent X with a g_{HXX} coupling, we get the departure $\delta T_{HHH}(s)$ due to the XXX triangle contribution to the HHH coupling:

$$\delta T_{HHH}(s) \to A_{XXX}(s) = -\frac{e\alpha}{4\pi} g^3_{HXX} C_0(s, m_H^2, m_H^2, m_X^2, m_X^2, m_X^2) \quad (19)$$

  where C_0 is the Passarino-Veltman [21] function. Using its high energy expansion [31] one gets (see (A.1))

$$-\frac{e\alpha}{4\pi} g^3_{HXX} \frac{\overline{\ln^2 s_X}}{2s} \quad , \quad (20)$$

  In the illustration we take $m_X = 0.5$ TeV and $g_{HXX} = -10$ TeV.

- for a fermionic constituent F, we get similarly the departure due to the FFF triangle

$$\delta T_{HHH}(s) \to A_{FFF}(s) = -\frac{e\alpha}{4\pi} g^3_{HFF} \Big\{ 2m_F^3 C_0 + 2m_F \Big[3m_H^2 (C_{21} + C_{22}) + 6p.p' C_{23}$$
$$+3nC_{24} + 2q.pC_{11} + 2q.p'C_{12} + 2m_H^2 C_{11} + 2p.p'C_{12} + q.pC_0 \Big] \Big\}$$
$$\to -\frac{e\alpha}{4\pi} g^3_{HFF} \{ 2m_F [\frac{-\overline{\ln^2 s_F}}{4} - \overline{\ln s_{FF}}] \} \quad , \quad (21)$$

  with the notations defined in eq.(A.1,A.2) of the Appendix. In the illustration we take $m_F = 0.5$ TeV and $g_{HFF} = -4$.

- and for a typical resonance effect we get the (trivial) shape

$$\delta T_{HHH}(s) \to A_{Res}(s) = \frac{g_{HR} g_{RHH}}{s - M_R^2 + i M_R \Gamma_R} \quad , \quad (22)$$

  The illustration is made with $M_R = 1$ TeV, $\Gamma_R = 0.3$ TeV, $g_{HR} g_{RHH} = 0.5$ TeV.

The numerical values of the above masses and effective couplings have been chosen such that, in the illustrations, the shape of the resulting HHH form factor can be quickly compared with that of the SM case such that one can appreciate the different spectacular s-dependencies. One indeed sees that the s dependencies appearing in these examples are very different from each other and also very different from the SM case.

So we believe that there is much to learn from the measurement of the HHH form factor.

We can now see how this reflects in the HV $\mu^-\mu^+ \to HH$ amplitudes (see Fig.4) and in the cross sections (see Fig.5) with their specific energy dependencies, threshold effects and resonance shapes.

In Fig.5 we show the relative differences $[\sigma_{SM+NP} - \sigma_{SM}]/\sigma_{SM}$ between the cross sections involving these new contributions and the pure SM cross sections, for the HV contribution (see (13)) and for unpolarized case. Due to the common dominating final $\delta T_{HHH}(s)$ term, the Left-Left and Right-Right HV cases defined in (13) would give similar results to the complete HV case. So one sees that polarized beams allowing the separation of HV from HC contributions would help for differentiating HHH form factor effects from possible other anomalous effects.

As one can see in the illustrations, the s and θ dependencies of the cross sections (even the unpolarized one) should allow to identify the nature of the new contribution.

At this point we should add a few words about the observability of such effects. The energy of a $\mu^-\mu^+$ collider has been considered up to 6 TeV [22]. For our study the required energy would correspond to the yet unknown new physics scale, although the curious anomalies observed at LHC around 0.75 and 2 TeV [23] could be in mind but it is too early to know how they would affect the HHH coupling.
With an expected luminosity of the order of $10^{35} cm^{-2} s^{-1}$ [22], the SM cross section (see Fig.2) would lead to only a few events per year. But we have seen that large enhancements could appear due to anomalous HHH couplings, threshold and resonance effects in the HHH form factor, which should then be observable. In case these luminosities could not be reached, we can mention that there may be other processes (for example WW fusion, see next Section) where HH production could be observed with a higher statistics, see for ex [24].

5 Conclusions

In this work we have computed the full 1-loop SM contributions to the $\mu^-\mu^+ \to HH$ process and we have studied the role of the final HHH coupling and of its SM form factor. Our aim is to show how possible new contributions to the HHH form factor could be identified through observables. We have emphasized the specific properties of the HC, HV amplitudes, their energy and angular dependencies and how this reflects in the observable polarized and unpolarized cross sections.

We have compared the real and imaginary parts of the SM 1-loop contributions to the HHH form factor, to examples of possible new physics effects corresponding either to Higgs boson compositeness or to the coupling of the Higgs boson to a new sector. In each case we have also given the corresponding simple analytic expressions, in the adequate "sim" approximation discussed in the Appendix and allowing a quick estimate of the effect at high s.

We have emphasized the fact that the $q^2 \equiv s$ dependencies of the HHH form factor can be very different, depending on their origin. We have taken some arbitrary cases with new scalar or new fermion contributions to the HHH form factor, or strong resonances, and made the corresponding illustrations. As it can be seen in these illustrations, the differences can be spectacular and reflect the specific nature of the new physics.

We have shown that polarized cross sections ($\mu^{\mp}$ beam polarization could be available according to some studies [15, 16]) are essential for differentiating HV contributions (which are the only ones containing HHH form factor effects) from HC contributions.

But even the shape of the s- and θ-dependencies of the unpolarized cross sections should help for identifying the nature of the new contribution.

The present study is an example of what could be done for the search of HHH form factor effects in the process $\mu^-\mu^+ \to HH$. Spectacular resonance or threshold effects could easily be seen but high luminosity would be required in order to make precise analyses. This would correspond to the simplest situation.

More complex processes like $ZZ \to HH$, $W^-W^+ \to HH$, $gg \to HH$ or $\gamma\gamma \to HH$ could be considered and would benefit of larger cross sections at e^-e^+, $\mu^-\mu^+$ colliders or at LHC. Note that the fusion subprocesses $ZZ \to HH$ and $W^-W^+ \to HH$ involve, like in the above $\mu^-\mu^+$ case, the simple s-channel H exchange diagram, with in addition a 4-leg $ZZHH$ or W^-W^+HH vertex, as well as t and u channel Z or W exchanges. These subprocesses can be measured by making detailed specific analyses.

The processes $gg \to HH$ and $\gamma\gamma \to HH$ contain an s-channel H exchange, but the initial vertex needs a 1-loop contribution and there are also several other 1-loop diagrams producing the final HH state. Specific works should be devoted to each of these processes, see e.g.[25, 26, 27, 28, 29].

The aim of this paper was only to to put forward the idea of looking especially at the s-dependence of the HHH form factor and to show that observable consequences may exist.

We hope that these first results will encourage further phenomenological and experimental studies of the possibilities to measure this form factor.

Appendix: SM contributions to the HHH form factor.

The SM prediction for the HHH form factor consists of a zero order contribution given by the point-like coupling g_{HHH} in (3), and of higher order corrections. In the OS scheme [18, 19] these corrections consist of parameter renormalization and additional 1-loop diagrams. We are interested in the $q^2 \equiv s$ dependence when one H is off-shell, while the two other H (with four-momenta p, p') are on-shell, in order to make the comparison of this SM prediction with possible compositeness structures.

So we will use a procedure allowing to quickly get simple forms which reflect sufficiently well the size and the s-dependence of each contribution. This is the supersimple renormalization scheme (SRS) procedure [20, 30], which leads to the simplest expressions in terms of augmented Sudakov logarithms. Among them, we will only need the augmented Sudakov forms (see [20, 30] for details):

$$\overline{\ln^2 s_X} \equiv \ln^2 s_X + 4L_{HXX} \quad , \quad s_X \equiv \left(\frac{-s-i\epsilon}{m_X^2}\right) \quad , \tag{A.1}$$

$$\overline{\ln s_{ij}} \equiv \ln s_{ij} + b_0^{ij}(m_H^2) - 2 \quad , \quad \ln s_{ij} \equiv \ln \frac{-s-i\epsilon}{m_i m_j} \quad , \tag{A.2}$$

where (X, i, j) refer to internal exchanges in the contributing diagrams. The explicit expressions for $b_0^{ij}(m_H^2)$ and L_{HXX} are given e.g. in (A.6, A.5) of [30]. We note that the counter terms needed in the SRS scheme respect the structure (A.1, A.2) [20, 30].

Globally this procedure consists in replacing the divergent terms related to the (i, j) internal lines of any contributing diagram, as

$$\ln \frac{-s-i\epsilon}{\mu^2} - \Delta \to \ln s_{ij} + b_0^{ij}(m_H^2) \quad , \tag{A.3}$$

where μ here denotes the renormalization scale and $\Delta = 1/\epsilon - \gamma_E + \ln(4\pi)$, with the number of dimensions used for regularization written as $n = 4 - 2\epsilon$.

In the present case, with only triangle and bubble diagrams contributing, there is no ambiguity related to the internal lines (i, j). They can only be H, Z, W and t, so that we can only have $(ij) = (HH), (ZZ), (WW), (tt)$. The SRS results thus obtained, are always denoted as "sim" in the illustrations [20, 30].

We next describe the exact expressions for the various triangle and bubble diagrams with 4-leg couplings, as well as their high energy SRS (sim) forms. At first α order, the $T^{SM}_{HHH}(s)$ form factor of (7), may be written as

$$T^{SM}_{HHH}(s) = e g_{HHH} + A^{SM}(s) \quad . \tag{A.4}$$

In the following two subsections we first give the $A^{SM}(s)$ results implied by the 1-loop triangles and bubbles with a 4-leg couplings, and then from the H self-energy.

A.1 Triangles and bubbles with 4-leg couplings

Depending on the natures of the exchanged particles, the contributions to $A^{SM}(s)$ from the various 2-point and 3-point Passarino-Veltman functions, denoted as B and C, are given by [21, 31]:

- **Scalar (SSS) triangles and (SS) bubbles with a 4-leg $SSHH$ coupling.**

$$\begin{aligned} A^{SM}_{SSS}(s) &= -\frac{e\alpha}{4\pi}\Bigg\{ g^3_{HSS} C_0(s, m_H^2, m_H^2, m_S^2, m_S^2, m_S^2) \\ &\quad + g_{HSS} g_{HHSS}\Big[B_0(s, m_S^2, m_S^2) + 2B_0(m_H^2, m_S^2, m_S^2\Big]\Bigg\} \\ &\to -\frac{e\alpha}{4\pi}\left\{ g^3_{HSS}\frac{\overline{\ln^2 s_S}}{s} - g_{HSS} g_{HHSS}\,\overline{\ln s_{SS}}\right\} \ . \end{aligned} \tag{A.5}$$

This applies to the triangles

$$SSS = HHH, G^0G^0G^0, C^ZC^ZC^Z, G^\pm G^\pm G^\pm, C^\pm C^\pm C^\pm \ ,$$

and the bubbles

$$SS = HH, G^0G^0, G^\pm G^\pm \ ,$$

while g_{HHH} is given in (3) and[2]

$$\begin{aligned} &g_{HHHH} = -\frac{3m_H^2}{4s_W^2 m_W^2} \ , \ g_{HGG} = -\frac{m_H^2}{2s_W m_W} \ , \ g_{HHGG} = \frac{1}{2s_W^2 c_W^2} \ , \\ &g_{HC^ZC^Z} = -\frac{m_W}{2s_W c_W^2} \ , \ g_{HC^\pm C^\pm} = -\frac{m_W}{2s_W} \ . \end{aligned} \tag{A.6}$$

Note that there is no 4-leg diagram for the ghost loop, and that a global fermionic minus sign has been inserted. In all cases, the internal S mass for $H, G^0, C^Z, G^\pm, C^\pm$ is respectively equal to the one of H, Z, Z, W, W.

- **Fermion triangles (fff).**
Due to the strong mass dependence of the Hff coupling, it is adequate to restrict to the $(ttt) + (\overline{ttt})$ case. The result is

$$\begin{aligned} A^{SM}_{ttt}(s) &= \frac{e\alpha}{4\pi}\frac{3m_t^3}{2s_W^3 m_W^3}\Bigg\{ 2m_t^3 C_0 + 2m_t[3m_H^2(C_{21}+C_{22}) + 6p.p' C_{23} \\ &\quad + 3nC_{24} + 2q.pC_{11} + 2q.p'C_{12} + 2m_H^2 C_{11} + 2p.p'C_{12} + q.pC_0]\Bigg\} \\ &\to \frac{e\alpha}{4\pi}\frac{3m_t^3}{2s_W^3 m_W^3}\left\{ 2m_t\left[\frac{-\overline{\ln^2 s_t}}{4} - \overline{\ln s_{tt}}\right]\right\} \ . \end{aligned} \tag{A.7}$$

[2] $(G^\pm, G^0)$ denote the SM Goldstone fields and $(C^\pm, C^Z)$ the FP ghosts.

- **Vector triangles** (VVV) **and bubbles** (VV) **with a 4-leg** $HHVV$ **coupling.**

$$A^{SM}_{VVV}(s) = \frac{e\alpha}{4\pi}\Big\{g^3_{HVV}nC_0 + g_{HVV}g_{HHVV}[2B_0(m_H^2, m_V^2, m_V^2) + B_0(s, m_V^2, m_V^2)]\Big\}$$
$$\to -\frac{e\alpha}{4\pi}\Big\{2g^3_{HVV}\frac{\overline{\ln^2 s_V}}{s} + g_{HVV}g_{HHVV}[-\overline{\ln s_{VV}}]\Big\} \quad , \tag{A.8}$$

applied only to $V = Z,\ W$, since there are no $HZ\gamma$ or $HHZ\gamma$ couplings. Because of this, the V masses in the SRS forms $\overline{\ln^2 s_V}$ and $\overline{\ln s_{VV}}$ can either be m_Z or m_W.

- (VVS) **triangles**

$$A^{SM}_{VVS}(s) = \frac{e\alpha}{4\pi}g^2_{VSH}g^2_{VVH}\Big\{m_H^2(C_{21} + C_{22}) + 2p.p'C_{23} + nC_{24}$$
$$+(p.p' + 3q.p)C_{11} + (m_H^2 + 3q.p')C_{12} + 2(q^2 + q.p')C_0\Big\}$$
$$\to \frac{e\alpha}{4\pi}g^2_{VSH}g^2_{VVH}\Big\{\frac{1}{2}(\overline{\ln^2 s_V} + \overline{\ln s_{VV}})\Big\} \quad , \tag{A.9}$$

applied to $ZZG^0,\ W^\pm W^\pm G^\pm$; compare (A.8).

- (VSV) **triangles**

$$A^{SM}_{VSV}(s) = \frac{e\alpha}{4\pi}g^2_{VSH}g^2_{VVH}\Big\{m_H^2(C_{21} + C_{22}) + 2p.p'C_{23} + nC_{24}$$
$$+(3m_H^2 - p.p')(C_{11} - C_{12}) + 2(m_H^2 - p.p')C_0\Big\}$$
$$\to \frac{e\alpha}{4\pi}g^2_{VSH}g^2_{VVH}\Big\{\frac{1}{4}\overline{\ln^2 s_V} + 2\overline{\ln s_{VV}}\Big\} \quad , \tag{A.10}$$

applied to $ZG^0Z,\ W^\pm G^\pm W^\pm$.

- (SVV) **triangles**

$$A^{SM}_{SVV}(s) = \frac{e\alpha}{4\pi}g^2_{VSH}g^2_{VVH}\Big\{m_H^2(C_{21} + C_{22}) + 2p.p'C_{23} + nC_{24}$$
$$-(m_H^2 + q.p)C_{11} - (p.p' + q.p')C_{12}) + q.pC_0\Big\}$$
$$\to \frac{e\alpha}{4\pi}g^2_{VSH}g^2_{VVH}\Big\{-\frac{1}{2}(\overline{\ln^2 s_V} + \overline{\ln s_{VV}})\Big\} \quad , \tag{A.11}$$

applied to $G^0ZZ, G^\pm W^\pm W^\pm$.

- (VSS) **triangles**

$$A^{SM}_{VSS}(s) = \frac{e\alpha}{4\pi} g^2_{VSH} g^2_{SSH} \Big\{ -m_H^2 (C_{21} + C_{22}) - 2p.p' C_{23} - nC_{24}$$
$$-2(m_H^2 + q.p) C_{11} - 2(p.p' + q.p') C_{12}) - 4q.p C_0 \Big\}$$
$$\to \frac{e\alpha}{4\pi} g^2_{VSH} g^2_{SSH} \Big\{ -\frac{1}{2} \overline{\ln^2 s_V} + \overline{\ln s_{VV}} \Big\} \ , \tag{A.12}$$

applied to $ZG^0G^0, W^\pm G^\pm G^\pm$.

- (SVS) **triangles**

$$A^{SM}_{SVS}(s) = \frac{e\alpha}{4\pi} g^2_{VSH} g^2_{SSH} \Big\{ -m_H^2 (C_{21} + C_{22}) - 2p.p' C_{23} - nC_{24}$$
$$-(-m_H^2 + q.p + p.p') C_{11} - (m_H^2 - p.p' + q.p') C_{12}) + (p.p' + q.p) C_0 \Big\}$$
$$\to \frac{e\alpha}{4\pi} g^2_{VSH} g^2_{SSH} \{ \overline{\ln^2 s_V} - \overline{\ln s_{VV}} \} \ , \tag{A.13}$$

applied to $G^0ZG^0,\ G^\pm W^\pm G^\pm$.

- (SSV) **triangles**

$$A^{SM}_{SSV}(s) = \frac{e\alpha}{4\pi} g^2_{VSH} g^2_{SSH} \Big\{ -m_H^2 (C_{21} + C_{22}) - 2p.p' C_{23} - nC_{24}$$
$$-(m_H^2 - q.p - p.p') C_{11} - (-m_H^2 + p.p' - q.p') C_{12}) + (-q.p' + q.p) C_0 \Big\}$$
$$\to \frac{e\alpha}{4\pi} g^2_{VSH} g^2_{SSH} \Big\{ -\frac{1}{2} \overline{\ln^2 s_V} + \overline{\ln s_{VV}} \Big\} \ , \tag{A.14}$$

applied to $G^0G^0Z,\ G^\pm G^\pm W^\pm$.

In the above contributions the following couplings are needed

$$g_{ZZH} = \frac{m_Z}{s_W c_W} \ , \ g_{ZZHH} = \frac{1}{2 s_W^2 c_W^2} \ ,$$
$$g_{WWH} = \frac{m_W}{s_W} \ , \ g_{WWHH} = \frac{1}{2 s_W^2} \ , \ g_{ZGH} = g_{WGH} = \frac{1}{2 s_W c_W} \ . \tag{A.15}$$

A.2 H self-energy

This additional contribution is given by

$$A_{se}^{SM}(s) = -\frac{e g_{HHH}}{s - m_H^2}\Sigma_H(s) \quad , \tag{A.16}$$

where $\Sigma_H(s)$ is computed from the following diagrams:

- **Bubbles** VV leading to

$$\Sigma_H(s) = \frac{X_1^2}{4\pi^2}[B_0] \to \frac{X_1^2}{4\pi^2}[-\overline{\ln s_{VV}}] \quad , \tag{A.17}$$

for which we respectively get

$$\begin{aligned} VV = ZZ \quad &\to \quad X_1^2 = \frac{e^2 M_W^2}{2 s_W^2 c_W^4} \quad , \\ VV = W^{\pm}W^{\mp} \quad &\to \quad X_1^2 = \frac{e^2 M_W^2}{s_W^2} \quad . \end{aligned} \tag{A.18}$$

- **Bubbles** SV leading to

$$\begin{aligned} \Sigma_H(s) \quad &= -\frac{X_1^2}{16\pi^2}[s(B_0 + B_{21} - 2B_1) + nB_{22}] \\ &\to -\frac{X_1^2}{16\pi^2}[-2s\overline{\ln s_{SV}}] \quad , \end{aligned} \tag{A.19}$$

for which we respectively get

$$\begin{aligned} SV = G^0 Z \quad &\to \quad X_1^2 = \frac{e^2}{4 s_W^2 c_W^2} \quad , \\ SV = G^{\mp}W^{\pm} \quad &\to \quad X_1^2 = \frac{e^2}{2 s_W^2} \quad . \end{aligned} \tag{A.20}$$

- **<u>Bubble</u>** <u>tt</u> leading to

$$\begin{aligned} \Sigma_H(s) &= -\frac{1}{4\pi^2}[(s(B_1 + B_{21}) + nB_{22} + m_t^2 B_0)X_1^2] \\ &\to -\frac{X_1^2}{4\pi^2}[\frac{s}{2}\overline{\ln s_{tt}}] \quad , \end{aligned} \tag{A.21}$$

with

$$X_1^2 = \frac{3e^2}{4 s_W^2 M_W^2}[m_t^2] \quad . \tag{A.22}$$

- **Bubbles** SS leading to

$$\Sigma_H(s) = \frac{X_1^2}{16\pi^2}[B_0] \to \frac{X_1^2}{16\pi^2}[-\overline{\ln s_{SS}}] \ , \tag{A.23}$$

with

$$X_1^2 = \frac{9e^2m_H^4}{8s_W^2M_W^2} \ , \ \frac{e^2m_H^4}{8s_W^2M_W^2} \ , \ \frac{e^2m_H^4}{4s_W^2M_W^2} \ , \ -\frac{e^2m_W^2}{4s_W^2c_W^4} \ , \ -\frac{e^2m_W^2}{2s_W^2} \ , \tag{A.24}$$

for

$$SS = \ \ HH, \ \ G^0G^0 \ , \ G^+,G^- \ , \ C^ZC^Z \ , \ C^+C^- \ \ , \tag{A.25}$$

respectively. Note that in these SS bubbles, the internal S mass is correspondingly equal to the mass of H, Z, W, Z, W.

References

[1] G. Aad *et al.* (ATLAS Collaboration), Phys. Lett. **B716**, 1 (2012). S. Chatrchyan *et al.* (CMS Collaboration), Phys. Lett. **B716**, 30 (2012), arXiv:1207.7235 [hep-ex]. Gavin J. Davies (CDF and D0 Collaborations), Front. Phys. China **8**, 270 (2013). ATLAS Collaboration: https://twiki.cern.ch/twiki/bin/view/AtlasPublic/HiggsPublicResults. CMS Collaboration: https://twiki.cern.ch/twiki/bin/view/CMSPublic/PhysicsResultsHIG.

[2] P. Higgs, Phys. Lett. **12**, 132 (1964); Phys. Rev. Lett. **13**, 508 (1964); Phys. Rev. **145**, 1156 (1966); F. Englert and R. Brout, Phys. Rev. Lett. **13**, 321 (1964); G. Guralnik, C. Hagen and T. Kibble, Phys. Rev. Lett. **13**, 585 (1964).

[3] S.L. Glashow, Nucl. Phys. **B22**, 579 (1961); S. Weinberg, Phys. Rev. Lett. **19**, 1264 (1967); A. Salam, Proc.8th Nobel Symposium,p.367 ed.N.Svartholm, Almqvist and Wiksell, Stockholm 1968.

[4] Ben Gripaios, arXiv:1503.02636, arXiv:1506.05039; A. Wulzer, arXiv: 1510.05159 (hep-ph).

[5] see A. Djouadi, Phys. Rept. **457**, 1 (2008) and arXiv: 1505.01059(hep-ph).

[6] G.F. Giudice, C. Grojean, A. Pomarol and R. Rattazzi, JHEP **0706**, 045 (2007).

[7] J. Ellis, V. Sanz and T. You, arXiv: 1410.7703(hep-ph).

[8] B.Patt and F. Wilczek, hep-ph/0605188.

[9] H. Terazawa, Y. Chikashige and K. Akama, Phys. Rev. **D15**, 480 (1977); for other references see H. Terazawa and M. Yasue, arXiv: 1508.00172(hep-ph); J. Mod. Phys. **5**, 205 (2014).

[10] D.B. Kaplan and H. Georgi, Phys. Lett. **136B**, 183 (1984). K. Agashe, R. Contino and A. Pomarol, Nucl. Phys. **B719**, 165 (2005): hep/ph 0412089.

[11] R. Contino, T. Kramer, M. Son, R. Sundrum, JHEP **0705**, 076 (2007).

[12] G. Panico and A. Wulzer, arxiv: 1506.01961 [hep-ph].

[13] M.E. Peskin, arXiv:1506.08185; M. Muhlleitner, arXiv:1410.5093.

[14] J. Baglio et al arXiv: 1212.5581; JHEP 1304(2013)151.

[15] D.B. Cline, N.I. A350(1994)26; V.D. Barger et al, Phys. Rept. **286**, 1 (1997), hep-ph/9602415; C. Rubbia, arXiv:1308.6612; Y. Alexahin et al,arXiv: 1308.2143; D. Neuffer et al, 1502.02042.

[16] D. Cline et al, hep-ph/9609002; B. Grzadkowski et al, hep-ph/0003091.

[17] G.J. Gounaris and F.M. Renard, Phys. Rev. Lett. **94**, 131601 (2005), Phys. Rev. **D73**, 097301 (2006).

[18] M. Böhm, H. Spiesberger, W. Hollik, Fortsch. Phys. **34**, 687 (1986); W. Hollik, Fortsch. Phys. **38**, 165 (1990); A. Denner, Fortsch. Phys. **41**, 307 (1993).

[19] A. Dobado, M.J. Herrero, W. Hollik and S. Peñaranda, Phys. Rev. **D66**, 2002 (095016).

[20] G.J. Gounaris and F.M. Renard, Acta Phys. Polon. **42**, 2107 (2011); Phys. Rev. **D86**, 013003 (2012); Phys. Rev. **D90**, 073007 (2014).

[21] G. Passarino and M. Veltman Nucl. Phys. **B160**, 151 (1979).

[22] J.P. Delahaye et al, arXiv:1502.01647 [physics-acc.ph].

[23] ATLAS note, ATLAS-Conf-2015-081; CMS note, CMS PAS EXO-15-004.

[24] A. Conway, H. Wentzel, E. Eichten and R. Lipton, arXiv 1405.5910 [hep-ex].

[25] R. Contino et al, JHEP **08**, 154 (2012); C-R Chen and I. Low, Phys. Rev. **D90**, 201 (013018). F. Goertz et al JHEP **04**, 167 (2015): A. Azatov et al arXiv:1502.00539.

[26] S.Dawson, A.Ismail and I.Low, Phys. Rev. **D91**, 115008 (2015).

[27] V.I. Telnov, JINST **9**,09(2014), arXiv:1409.5563.

[28] E. Asakawa *et al*,, arXiv: 1009.4670; Phys. Rev. **D82**, 115002 (2010).

[29] A. Levy, CLICdp-Conf-2015-001, arXiv:1501.02614.

[30] G.J. Gounaris and F.M. Renard, Phys. Rev. **D88**, 113003 (2013).

[31] M. Beccaria, G.J. Gounaris, J. Layssac and F.M. Renard, Int. J. Mod. Phys. **A23**, 1839 (2008).

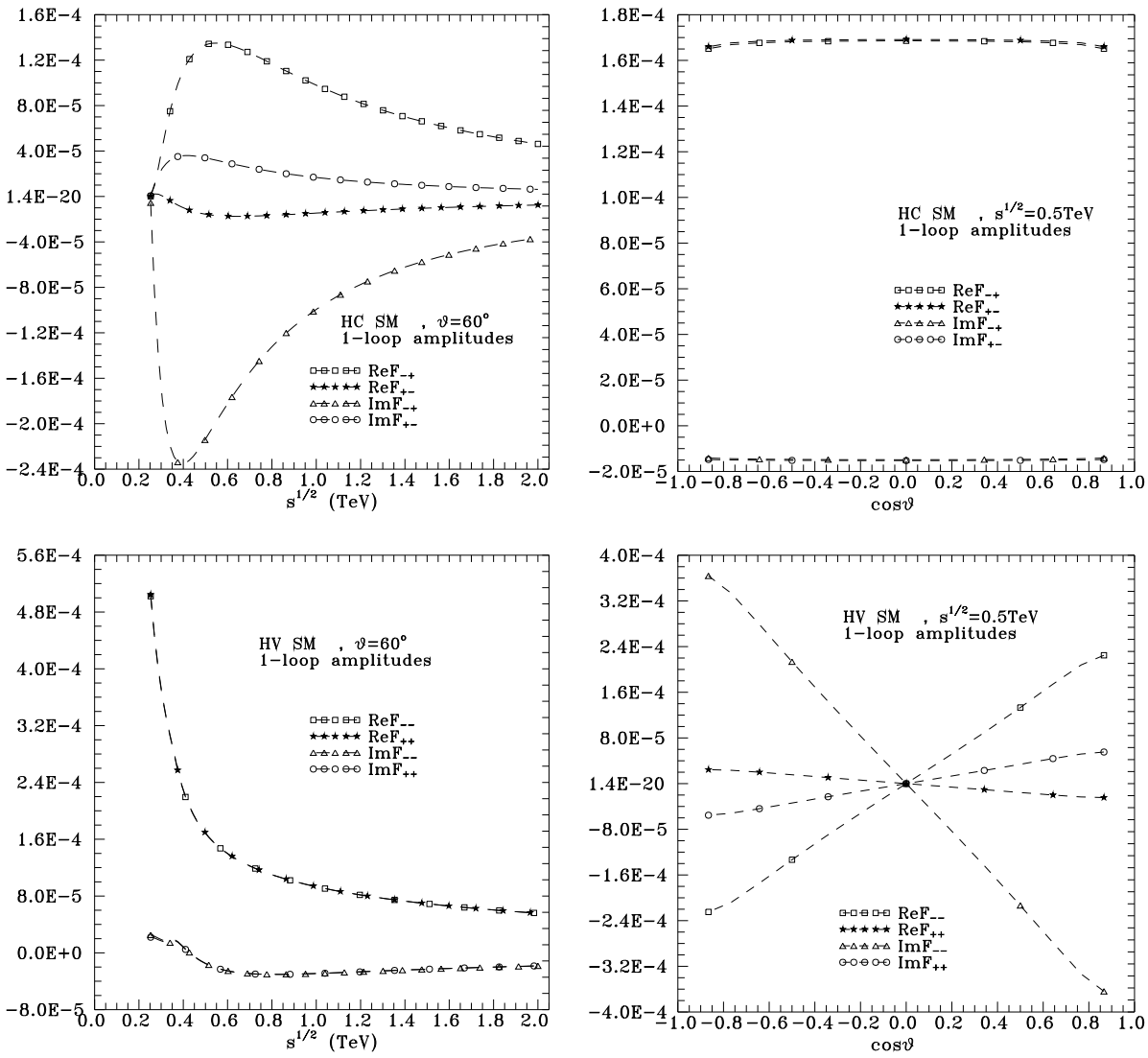

Figure 1: The complete SM 1-loop HC amplitudes (upper panels) and the corresponding HV amplitudes (lower panels). Left panels present the energy dependencies at $\theta = 60°$, while right panels the angular dependencies at $\sqrt{s} = 0.5$TeV.

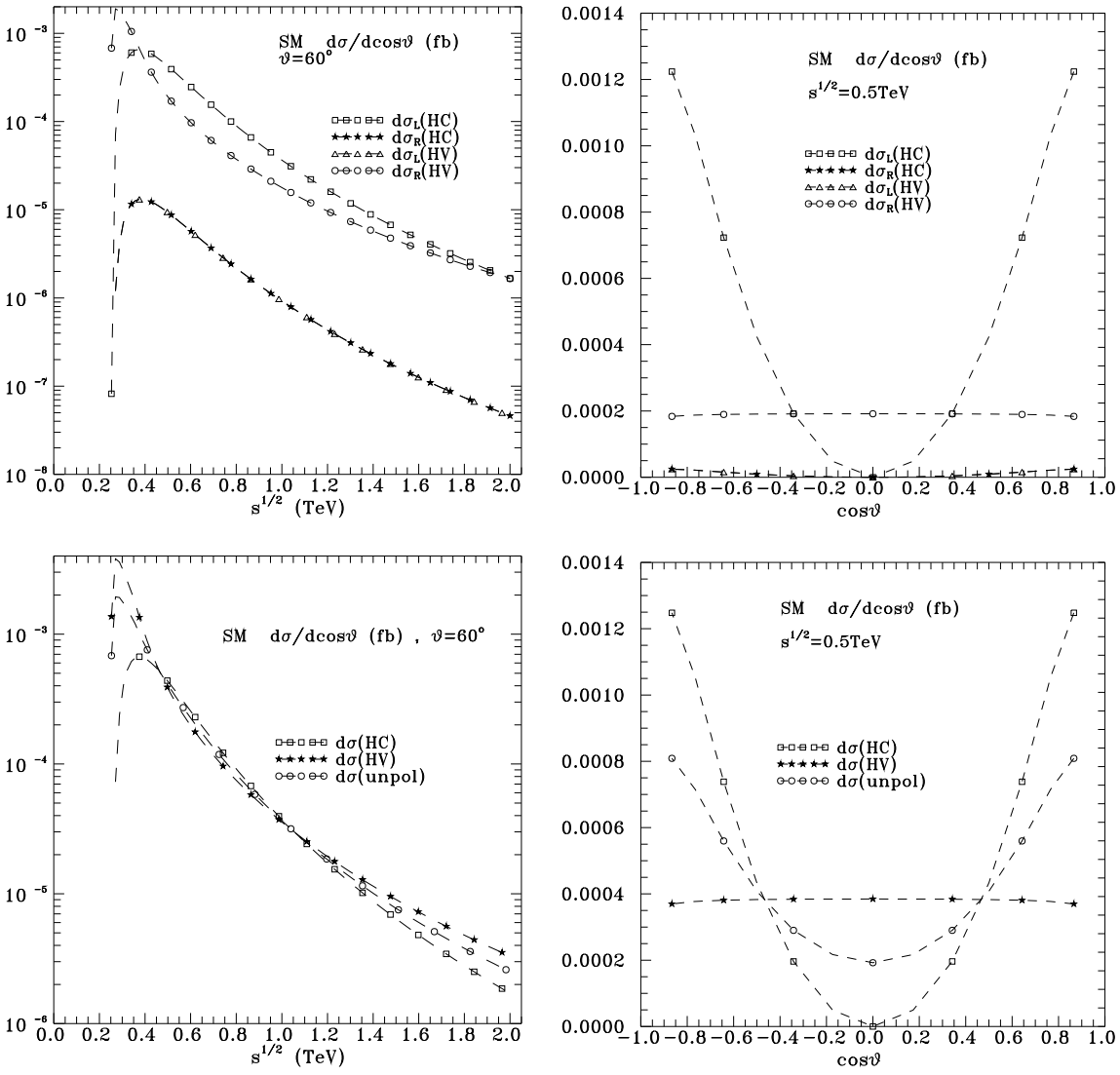

Figure 2: SM 1-loop differential cross sections as defined in (13, 14). Left panels present the energy dependencies at $\theta = 60°$, while right panels the angular ones at $\sqrt{s} = 0.5$TeV.

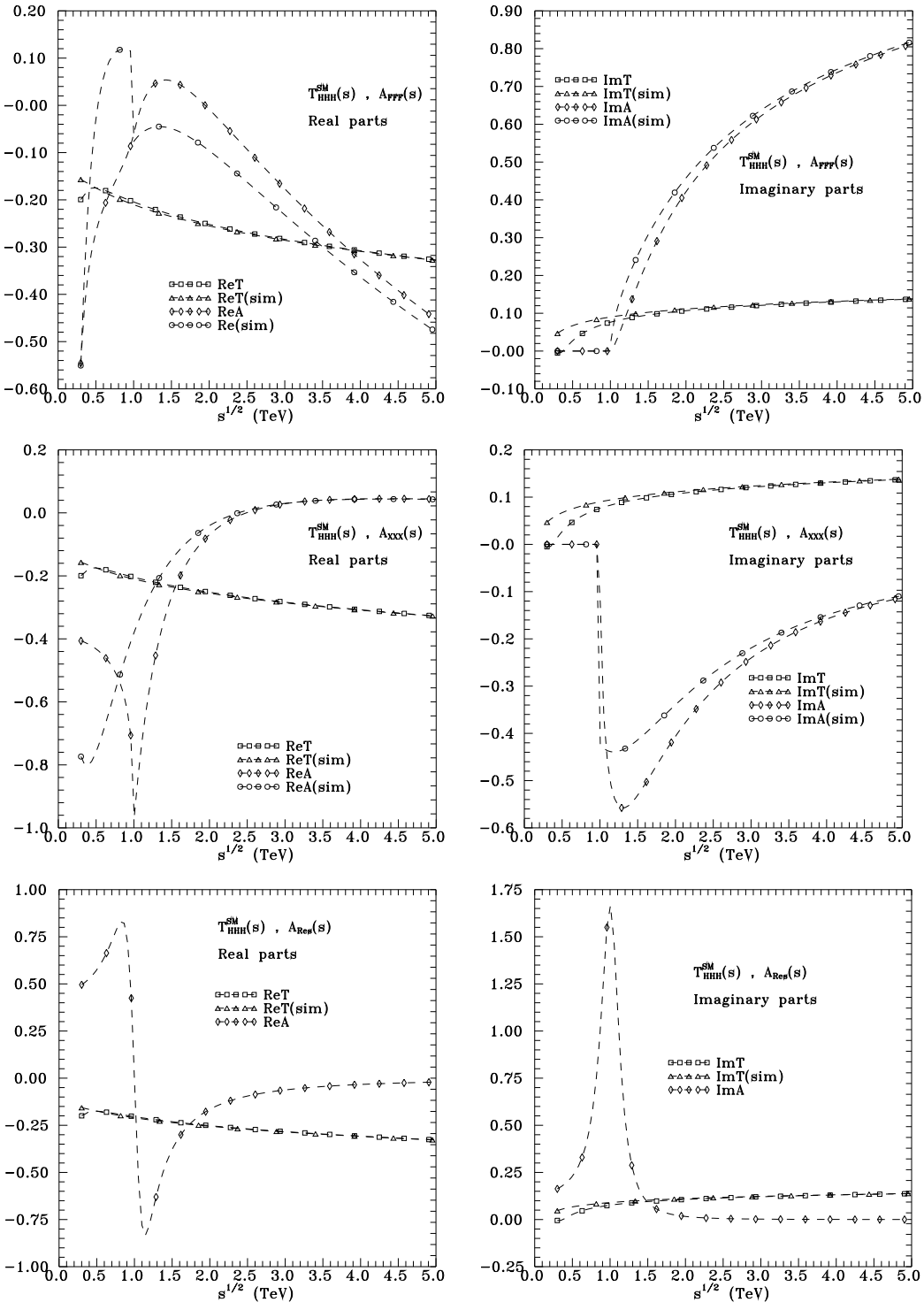

Figure 3: The s-dependence of SM form factor T^{SM}_{HHH} defined in (7), together with the new physics contributions to it from $A(s)_{FFF}$ of (21) (upper panels), $A(s)_{XXX}$ of (20) (middle panels), and $A(s)_{\rm Res}$ of (22) (lower panels). Left and right panels present real and imaginary parts respectively. T refers to the SM contribution, A to the new physics contributions, with the following parameters $m_X = 0.5$ TeV and $g_{HXX} = -10$ TeV, $m_F = 0.5$ TeV and $g_{HFF} = -4$, $M_R = 1$ TeV, $\Gamma_R = 0.3$ TeV, $g_{HR}g_{RHH} = 0.5$ TeV. The supersimplicity (SRS) predictions given in (A.1, A.2) are denoted T(sim).

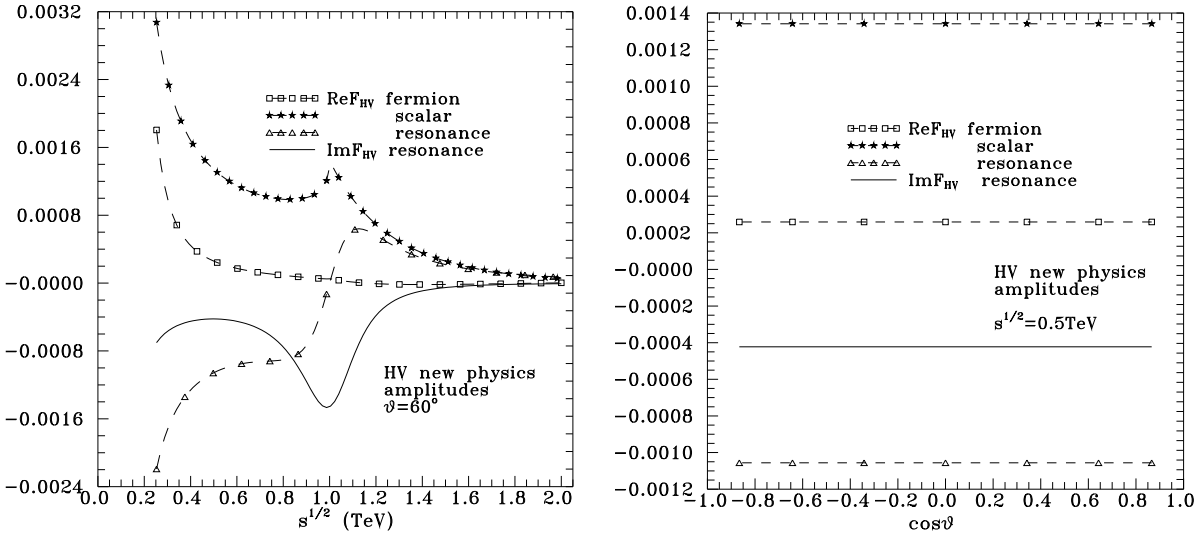

Figure 4: The New Physics contributions to the HV amplitudes induced by the HHH form factors of Fig.3. The HC amplitudes and the imaginary parts in the "new fermion" and "new scalar" HV amplitudes are vanishing and they are not shown. Left panel presents the energy dependencies, while the right panel the angular ones, as in Fig.1.

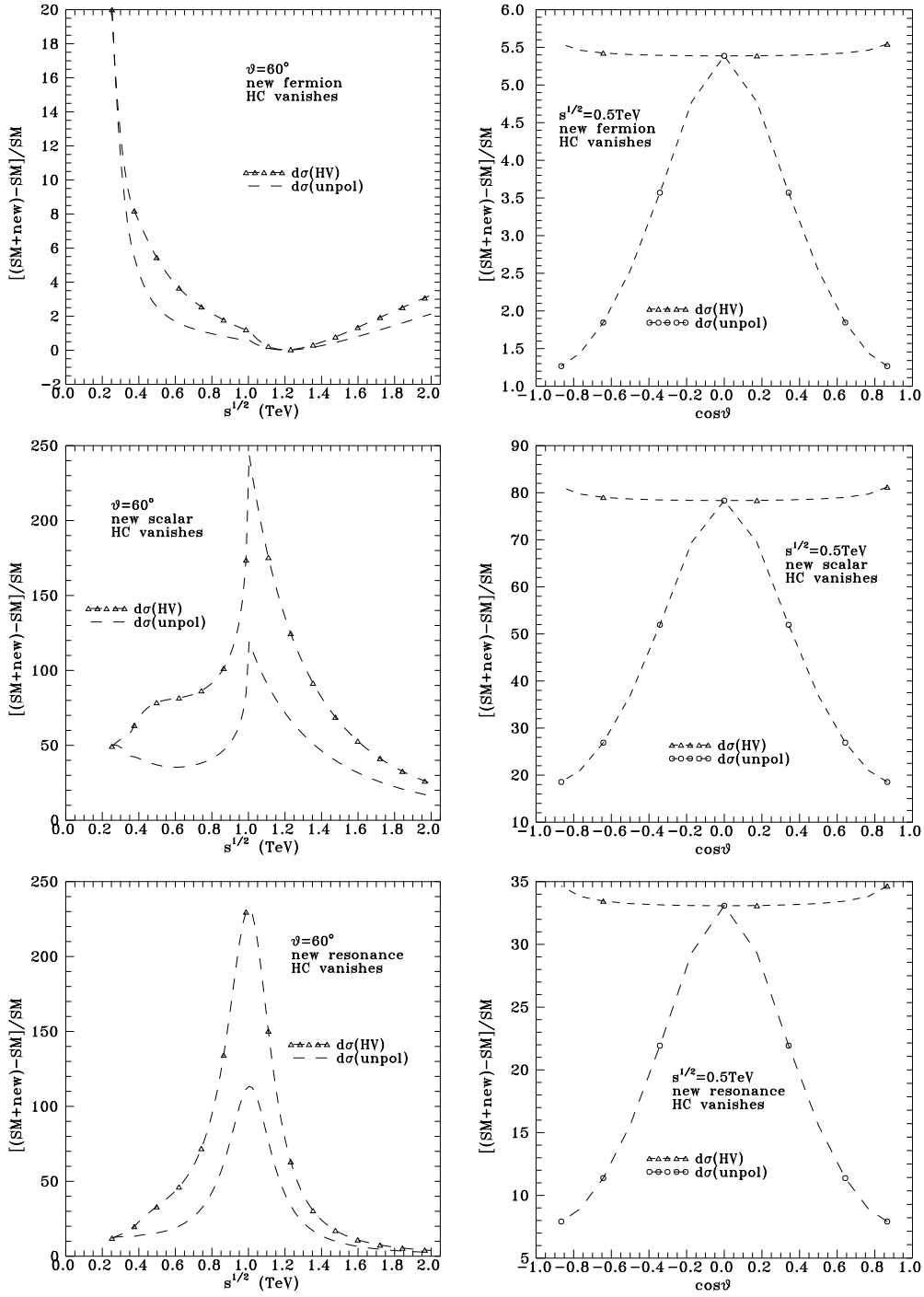

Figure 5: Dependencies of $[d\sigma(SM + \text{new})/d\cos\vartheta - d\sigma(SM)/d\cos\vartheta]/[d\sigma(SM)/d\cos\vartheta]$, on the "new fermion" (upper), "new scalar" (middle) and the "new resonance" (lower panel) contributions for the total HV case in (13) and for the unpolarized case.